International Journal of Architectural, Civil and Construction Sciences
ISSN: 2415-1734
Vol:10, No:1, 2016

Monitoring the Drying and Grinding Process during Production of Celitement through a NIR-Spectroscopy Based Approach

Carolin Lutz, Jörg Matthes, Patrick Waibel, Ulrich Precht, Krassimir Garbev, Günter Beuchle, Uwe Schweike, Peter Stemmermann, Hubert B. Keller

Abstract**—**Online measurement of the product quality is a challenging task in cement production, especially in the production of Celitement, a novel environmentally friendly hydraulic binder. The mineralogy and chemical composition of clinker in ordinary Portland cement production is measured by X-ray diffraction (XRD) and X-ray fluorescence (XRF), where only crystalline constituents can be detected. But only a small part of the Celitement components can be measured via XRD, because most constituents have an amorphous structure. This paper describes the development of algorithms suitable for an on-line monitoring of the final processing step of Celitement based on NIR-data. For calibration intermediate products were dried at different temperatures and ground for variable durations. The products were analyzed using XRD and thermogravimetric analyses together with NIR-spectroscopy to investigate the dependency between the drying and the milling processes on one and the NIR-signal on the other side. As a result, different characteristic parameters have been defined. A short overview of the Celitement process and the challenging tasks of the online measurement and evaluation of the product quality will be presented. Subsequently, methods for systematic development of near-infrared calibration models and the determination of the final calibration model will be introduced. The application of the model on experimental data illustrates that NIR-spectroscopy allows for a quick and sufficiently exact determination of crucial process parameters.

Keywords**—**Calibration model, celitement, cementitious material, NIR spectroscopy.

I. Introduction

THE cement sector is one of the industries with a very high energy consumption and carbon dioxide emission. With estimated annual CO_2 emissions of around 3.5 billion tons, the cement production has a global share of about 9.5-10 % [1]. At the Karlsruhe Institute of Technology (KIT) a new environmentally friendly process for the production of a novel hydraulic binder (Celitement), comparable to ordinary Portland cement (OPC), with a high potential for saving energy and reducing carbon dioxide emissions was invented. With a lower demand of limestone and significantly lower temperatures, the new process has the potential to save up to 50 percent of the energy consumption compared to OPC. Celitement is produced from limestone and sand in a two-stage process. The first step is a hydrothermal synthesis in an autoclave, but the intermediate product is not yet hydraulically active. After drying, the intermediate product is activated to hydraulic calcium hydrosilicate through a dedicated reaction grinding [2]. Until now an online measurement and evaluation of the product quality in the manufacturing process has not been realized. Only complex or time consuming analytical methods such as X-ray diffraction (XRD), thermogravimetric analyses or the determination of the compressive strength after hydration allow for a quantification of the product quality. Additionally, Celitement has a high share of amorphous phases, which cannot be detected by XRD. In the future, an online-near-infrared (NIR)-spectroscopy measurement system should allow for a reliable monitoring of the product quality after the reaction grinding. NIR-spectroscopy was selected due to its simplicity, performance and robustness. Chemometric methods with NIR are well established for other non-cementitious applications and can allow for a quantification of physical and chemical parameters.

A. The Celitement Process

Celitement is based on the same raw materials as ordinary Portland cement (OPC) and also the reaction with water is similar, but the production process is completely different. Fig. 1 demonstrates the process stages of the Celitement production. The first process step is the same as in OPC production. Calcium carbonate is calcined to calcium oxide. After deacidification calcium oxide is mixed with silicon dioxide and water for further processing. At temperatures between 140°C and 300°C various calcium silicate hydrates (CSH-phases) are formed in an autoclave. These phases are already structurally related to the final product, but not hydraulically active yet. They are stabilized by hydrogen bonds and are not able to react with water.

Carolin Lutz is with the Institute for Applied Computer Science at the Karlsruhe Institute of Technology, Karlsruhe, Germany (phone: +49 721 608 28429; fax: +49 721 608 25702; e-mail: carolin.lutz@kit.edu).

Jörg Matthes, Patrick Waibel and Hubert B. Keller are with the Institute for Applied Computer Science at the Karlsruhe Institute of Technology, Karlsruhe, Germany (e-mail: joerg.matthes@kit.edu, patrick.waibel@kit.edu, hubert.keller@kit.edu).

Ulrich Precht, Krassimir Garbev, Günter Beuchle, Uwe Schweike and Peter Stemmermann are with the Institute for Technical Chemistry at the Karlsruhe Institute of Technology, Karlsruhe, Germany (e-mail: ulrich.precht@kit.edu, krassimir.garbev@kit.edu, guenter.beuchle@kit.edu, uwe.schweike@kit.edu, peter.stemmermann@kit.edu).

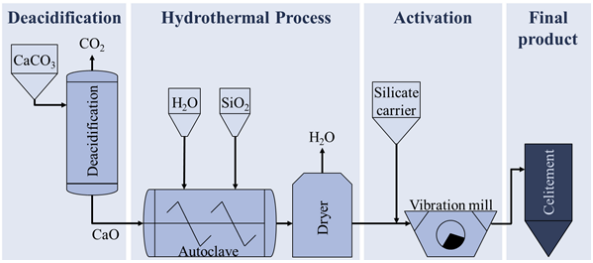

Fig. 1 Overview of the process steps in Celitement production

The material is then dried in the autoclave or in a cabinet dryer for the removal of excess water. In the future, on an industrial scale a more energy efficient drying process with a process control based on online measurements will be established. Therefore, it is necessary to examine the drying process and especially the drying temperature, in order to determine how it influences the final product quality. Additionally, it is interesting to survey the drying process in relation with the subsequent grinding process, where the CSH-phases are activated. In the activation step the hydrogen bonds of the hydrothermal precursor are modified. Hence, a silicon oxide carrier is added and ground together with the hydrothermal precursor in a vibratory ball mill. This leads to reorganization of the product structure and also to an amorphization and partial breakage of the hydrogen bonds. New fragments are shaped, which consist of hydrosilicates accumulated on the carriers surfaces in form of a reactive shell over the inert core. The formed calciumhydrosilicates (CHS-phases) are hydraulically active and allow formulation of mortars or concrete just as OPC. [2]-[4] However, until now monitoring the product quality of Celitement, especially during the production process, is a difficult task. Due to the amorphous content of the intermediate and the final product, analytical methods such as XRD and XRF, which are well established for the monitoring of OPC production, can only partially be used. Additional thermogravimetric analyses and measurement of the compressive strength of mixed mortars are necessary to assess the product quality, but both methods are time-consuming. The combination of all these analytical techniques results in a good knowledge about the product quality. For a production on the industrial scale a measurement system is necessary, which allows for a faster detection and estimation of composition and quality during processing.

B. Monitoring of the Drying and Grinding Process Steps

The basic idea is to use a NIR-spectrometer and associated calibration models to calculate some crucial parameters which are significant for the products quality. This shall result in an online estimation of quality parameters after the grinding process. Goal of the grinding process is activation of the intermediate material rather than particle size reduction. Therefore, particle size analysis is not suitable for monitoring the progress of the grinding. For a reliable selection of crucial parameters different process steps need to be analyzed. Therefore, the variation of the product in an experimental series of different drying temperatures and grinding durations is explored using existing analytical techniques and additionally NIR-spectroscopy. In Section II, the experimental setup, the measurement systems and the methods will be described as well as some of the parameters. Subsequently, exemplary results of the parameter measurement, the calculation of calibration models and the relation to the measured compressive strength of the mortar, the drying temperature and the grinding duration will be presented.

II. Experimental Setup

The basic idea of the experimental series is the examination of the drying and the grinding process steps at laboratory size. One batch (around 60 kg) of intermediate product was produced in the autoclave of the pilot plant and stored hermetically sealed. This batch was used for all experiments to ensure comparability. Samples were dried in a small laboratory cabinet dryer at different temperatures and ground for variable durations in a laboratory vibration mill with a capacity of roughly 1 kg material.

The samples in the experimental series were dried until all nine thermocouples distributed in the sample reached a constant temperature close to the temperature of the cabinet dryer. Each sample weighted 6 kg before drying. The samples were dried at 150°C, 170°C, 190°C, 210°C, 230°C, 250°C and 290°C. After drying, around 70 to 75% of the mass remained. The dried samples were divided into four parts, each weighing around 1 kg. One sample was analyzed without grinding and the other three samples were ground for one, three and six hours, respectively. After the grinding process, the samples were analyzed by XRD, thermogravimetric analysis and NIR-spectroscopy. Additionally, the compressive strength and the tensile strength were determined on standard mortar prisms after 1, 2, 7 and 28 days of hydration.

In addition to the compressive strength, the product quality of Celitement is mainly assessed based on XRD measurements including the application of the Rietveld method [5]. Using these measurements it is possible to determine the weight fraction and the crystallite size of the crystalline constituents and the overall weight fraction of the X-ray-amorphous components. In this paper an approach to the direct determination of crucial parameters from NIR-spectra is introduced. Detailed results for three parameters are presented:

- The fraction of X-ray-amorphous material in the sample (*Amorphous*) is the weight fraction of components, which are not detected by XRD.
- *Calcite* (calcium carbonate) is a remainder of the raw material. It is a very soft material and can easily be ground. Hence, it can also provide an indication of the grinding progress.
- *Alpha* represents the weight fraction of α-$Ca_2[HSiO_4]OH$ (α-C_2SH) in the sample. *Alpha* is produced in the autoclave and reduced during grinding. Its reduction can be considered as an indication of the progress of the grinding process.

The parameter *Sum-CSH-CHS* - which is the total share of the CSH and CHS phases in the product – is obtained by

thermogravimetric analyses and will be investigated as well.

The NIR-spectra were measured using a FT-NIR-spectrometer MATRIX-F (Bruker Optics, Ettlingen, Germany), which is suitable for the dusty environment occurring in the Celitement production. The Spectra were recorded in the diffuse reflectance mode in the range 4000-12000 cm^{-1}, using a resolution of 8 cm^{-1} and the average of 32 scans with a handheld reflection probe IN261 (Bruker Optics, Ettlingen, Germany) [6]. For recording, the sample is mixed and slightly compacted, the reflection probe is immersed and the scans are started while applying a small amount of pressure with the probe onto the sample. The result is a set of two average NIR-spectra per sample based on 32 scans each. The NIR-spectra are used as training data set for calculating calibration models for the parameters. Finally the direct calculation of the parameters from the measured NIR-spectra shall be possible.

III. Methods

A. Pre-Treatment

For processing, the NIR-spectra are exported to MATLAB (MathWorks Inc, USA), where the calculation of the calibration model and the application to new data is executed. The calculation of the calibration model is developed for different combinations of data pre-processing steps, different ranges in the spectra and several model orders a. The training data set consists of the matrix of NIR-spectra $\boldsymbol{X} \in \mathbb{R}^{M \times N}$ containing the single spectra $\boldsymbol{x}_i$, where i indicates the specific spectrum, and a column vector $\boldsymbol{y} \in \mathbb{R}^{N}$ containing the particular selected measured parameter. M represents the number of wavenumbers and N the number of NIR-spectra.

The spectra are pre-treated in order to reduce noise and other disturbing effects and to accentuate the desired characteristics. There are two kinds of data pre-treatment. While the optional methods can be used and combined in different variations, one of the following two mandatory pre-treatments is required for the implementation of partial-least-squares-regression (PLSR) to calculate the calibration model:

- For column-centering the spectra are mean-adjusted for each wavenumber by;

$$\boldsymbol{x}_{i,cc} = \boldsymbol{x}_i - \mathbf{1}_N \cdot x_{mean} \tag{1}$$

with x_{mean} as the average value of the whole spectrum i and $\boldsymbol{x}_{i,cc}$ the column-centered spectrum.

- For the multiplicative scatter correction (MSC) each spectrum $\boldsymbol{x}_i$ is adjusted by stretching and shifting with the approach;

$$\boldsymbol{x}_{i,MSC} = \frac{\boldsymbol{x}_i - a_i}{b_i}, \tag{2}$$

where $\boldsymbol{x}_{i,MSC}$ represents the MSC-corrected spectrum and a_i and b_i the coefficients. With the approach;

$$\left\| \boldsymbol{x}_{i,MSC} - \bar{\boldsymbol{x}} \right\|_2^2 \rightarrow \min_{a_i,b_i} \tag{3}$$

The aim is to fit the spectrum as good as possible to the average spectrum $\bar{\boldsymbol{x}}$ of the training data set. The coefficients a_i and b_i can be calculated with;

$$\left\| [\mathbf{1}_N \quad \bar{\boldsymbol{x}}] \begin{bmatrix} a_i \\ b_i \end{bmatrix} - \boldsymbol{x}_i \right\|_2^2 \rightarrow \min_{a_i,b_i} \tag{4}$$

or dissolved with least-squares:

$$\begin{bmatrix} a_i \\ b_i \end{bmatrix} = \left[\begin{bmatrix} \mathbf{1}_N^T \\ \bar{\boldsymbol{x}}^T \end{bmatrix} [\mathbf{1}_N \quad \bar{\boldsymbol{x}}] \right]^{-1} \begin{bmatrix} \mathbf{1}_N^T \\ \bar{\boldsymbol{x}}^T \end{bmatrix} \boldsymbol{x}_i \tag{5}$$

for each measured NIR-spectrum individually. [7], [8].

The integrated optional pre-treatment of the spectra, which can be used in different combinations, are:

- The moving average filter (MA) for reducing superposed trends [7], [8].
- The first derivative spectrum for removing baseline effects and to increase spectral resolution [7], [8].
- The limitation of the data to a certain wavenumber range for reducing noise in the regions of very large and very small wavenumbers [8].
- The standard normal variate (SNV) transformation for applying additional correction of scattering effects caused by variation of particle size [9].

An additional pre-treatment of the data is the subdivision of the spectrum into several spectral ranges, because it is not necessary to include the whole spectrum in the calculation of the calibration model. Calibration models are then calculated for all possible combinations of the spectral ranges. The combination with the best result for the calibration model is selected. Thus spectral ranges without significant information on the sample and regions of noisy data are neglected [10].

Besides the pre-treatment of the spectra, it can also be advantageous to examine the target vector containing the parameter. The mean-adjustment of the target-vector is a mandatory pre-treatment as well. Additionally, the target vector can be adjusted by calculating the conversion rate of the parameter, if the initial value of the parameter is known. The conversion rate $y_{i,cr}$ can be calculated with;

$$y_{i,cr} = 1 - \frac{y_i}{y_0} \tag{6}$$

where y_i is the absolute measured target value and y_0 the initial value before grinding. When applying the calibration model to a new data set with known initial value, it is possible to recalculate the absolute value of the parameter, but also without recalculation, the conversion rate can give information about the progress of the grinding process. The idea behind this pre-treatment is the improvement of parameters, which have a wide range in composition and high fluctuations in the initial value. Depending on the raw material and the process adjustments, the composition of the intermediate product from the hydrothermal process can vary and consequently also the gradient of the parameter during grinding is variable. With the application of the conversion rate it is tried to linearize these information of the parameters with different initial values and

different formation or reduction rates in conjunction with the NIR-spectra [10].

B. Partial-Least-Squares

The focus in the calculation of the calibration model is on the standard procedure of iterative partial-least-squares-regression (PLSR). Therefore, it is emanated from a linear approach;

$$\boldsymbol{y} = \boldsymbol{X}\boldsymbol{b}_1 + \mathbf{1}_N b_0 + \boldsymbol{e} \tag{7}$$

where $\boldsymbol{b} = \begin{bmatrix} b_0 \\ \boldsymbol{b_1} \end{bmatrix}$ constitutes the calibration model and $\boldsymbol{e}$ a zero-mean Gaussian noise vector with the deviations. The equation can be transferred to;

$$\|\boldsymbol{X}\boldsymbol{b} - \boldsymbol{y}\|_2^2 \rightarrow \min_{\boldsymbol{b}} \tag{8}$$

and resolved for vector $\boldsymbol{b}$ according to the least-squares method to;

$$\boldsymbol{b}_{LS} = (\boldsymbol{X}^T\boldsymbol{X})^{-1}\boldsymbol{X}^T\boldsymbol{y} \tag{9}$$

with $\boldsymbol{X}$ containing the pre-treated NIR-spectra and $\boldsymbol{y}$, the pre-treated target-vector. In this case, for the calculation of the calibration model, this equation is not solvable as $\boldsymbol{X}$ does not have full column rank. The idea of the PLSR is the reduction of the dimensions of $\boldsymbol{X}$ to a model order $a \leq N$. For that purpose a weighting matrix $\boldsymbol{W} \in \mathbb{R}^{M \times a}$ referring to a scores matrix $\mathbf{T} = \mathbf{XW}$ is calculated for the dimension reduction. The determination of the weighting and the scores matrixes is executed by iteration. In the end, the calibration model can be calculated with;

$$\mathbf{b}_{\mathrm{PLS}} = \mathbf{W}(\mathbf{W}^{\mathrm{T}}\mathbf{X}^{\mathrm{T}}\mathbf{X}\mathbf{W})^{-1}\mathbf{W}^{\mathrm{T}}\mathbf{X}^{\mathrm{T}}\mathbf{y} \tag{10}$$

The calibration model $\boldsymbol{b}_{PLS}$ consists of a vector, which can be directly applied to a new spectrum for the calculation of the associated parameter. Of course the data pre-treatment used for the calibration model has to be applied to the new spectrum before. [11], [12].

C. Validation and Evaluation

The calibration model is calculated for all possible combinations of the pre-treatment methods, for all possible combinations of the spectral ranges and for all model orders a up to the selected maximal order. For each possible combination the cross-validation as leave-one-out procedure is applied as internal validation. The coefficient of determination (R^2) can be estimated with the calculated and measured parameters [10]. The calibration model with the highest value for the coefficient of determination is selected. The first step is the selection of the best model order for each combination of the data pre-treatment and combination of the spectral ranges. Therefore, the deviations between the different model orders for the coefficient of determination are compared. The model order with the last high increase (depending on the variations between more than 0.5 and 1% of R^2) before reaching the maximum coefficient is selected in order to keep the model complexity as low as possible and as high as needed. For each combination of data pre-treatment, the combination of the spectral ranges with the highest coefficient of determination is selected. In the end all combinations of data pre-treatment are compared and the combination with highest coefficient of determination is selected as long as the coefficient of determination is less than 2.5% improvement for the next higher model order.

IV. Results

The data set consists of the described 28 experiments with seven different drying temperatures and four different grinding durations per temperature (Table I). On the one hand the measurements are the NIR-spectra and on the other hand the parameters measured either with XRD or thermogravimetric analysis as outlined in Section II. Additionally, the compressive strength is measured for all grinded samples following the standardized procedure of DIN EN 12390-2 for production and storage of standardized mortar prims [13]. In the next paragraph, the dependence of these parameters on drying temperature and grinding duration is presented. Subsequently, some results of the calculation of calibration models for the belonging NIR-spectra and presented parameters are illustrated.

A. Analysis of Parameters and Compressive Strength

Different parameters have been measured by XRD (exemplarily *Amorphous* and *Calcite*) and thermogravimetric analysis (e.g. *Sum-CSH-CHS*). Figs. 2-4 show the dependency of the parameters on drying temperatures and grinding durations, respectively.

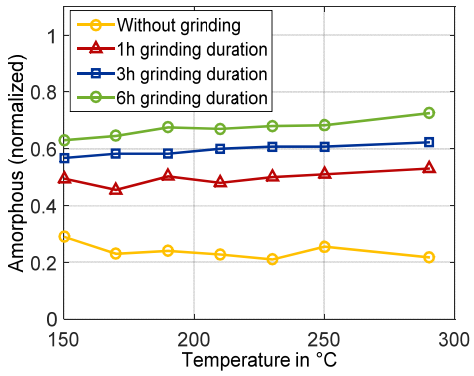

Fig. 2 Change of *Amorphous* with increasing drying temperature for different grinding durations

Amorphous is the weight fraction of amorphous material in the sample. The hydraulically active constituents, activated by grinding, are included in the amorphous fraction. This means, the increase of this weight fraction probably shows a concurrent increase of the fraction of the hydraulically active material. Thus, one aim of the grinding process is an increase in the share of amorphous material. Fig. 2 shows that the influence of the grinding process on the weight fraction of

Amorphous is significantly higher than the influence of the drying temperature. However, *Amorphous* is slightly increasing with the drying temperature and noticeably increasing with the grinding duration. Looking at *Amorphous*, there is probably a slight improve for the grinding process with the thermal treatment of the intermediate product.

The weight fraction of *Calcite* shows only small variations with varying drying temperature (Fig. 3). The dependency on the grinding duration appears much more clearly. Initially, the share of *Calcite* is slightly higher after one hour grinding and then decreases to half or even to a quarter of the previous value for three and six hours of grinding duration. *Calcite* is a very soft material and can also be an indicator of the grinding progress.

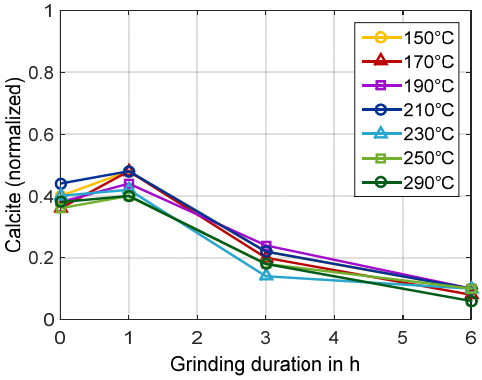

Fig. 3 Change of *Calcite* with increasing grinding duration for different drying temperatures

The CHS-phase is responsible for the solidification of the cement. During hydration the CHS-phases react to CSH-phases. A small proportion of CSH-phases is already contained in the product. Combined they can indicate the potential of the product, where the quality is better for increasing share of *Sum-CSH-CHS*. This parameter is obtained by thermogravimetric analysis, which is very time consuming. Fig. 4 illustrates the dependency of *Sum-CSH-CHS* on drying temperature and grinding duration. There is no noticeable correlation of the drying temperature and the share of *Sum-CSH-CHS*. The grinding duration, on the other hand, has a strong effect. With increasing grinding duration the *Sum-CSH-CHS* is increasing, where four samples reach their maximum after three hours of grinding and two samples after six hours. This parameter can represent the activation during the grinding process, where the CHS-phases are formed.

The dependence of the compressive strength on drying temperature and grinding duration is shown in Fig. 5. It is significantly higher for a lower grinding duration of one hour and very similar for three and six hours of grinding after one day and noticeable lower after 28 days of hydration. The drying temperature affects the compressive strength after one day of hydration as well. With increasing drying temperature the compressive strength is slightly decreasing for one hour grinding. For longer grinding the decrease is considerably higher. After 28 days of hydration the differences between the drying temperatures have disappeared and higher compressive strength corresponds to higher grinding duration.

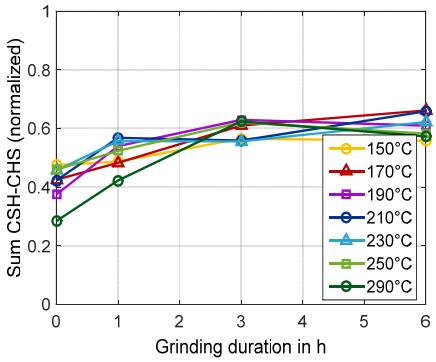

Fig. 4 Change of *Sum-CSH-CHS* with increasing grinding duration for different drying temperatures

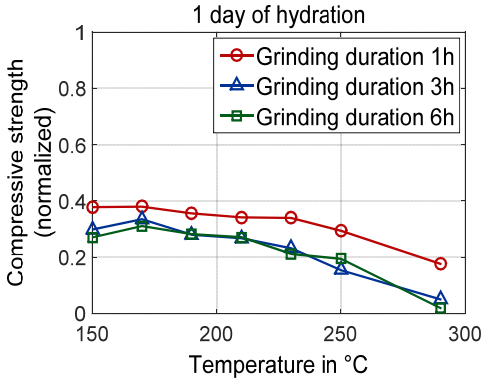

(a)

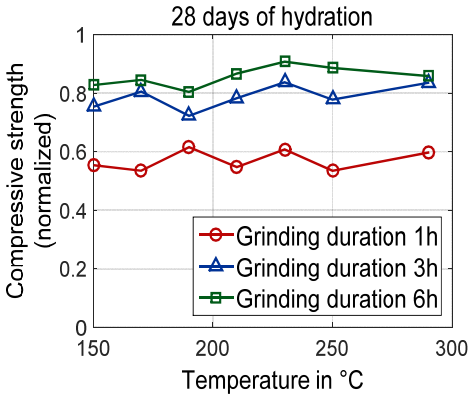

(b)

Fig. 5 Compressive strength for different drying temperatures and different grinding durations (a) after one day of hydration time and (b) after 28 days of hydration time

The dependency of the parameters *Amorphous* and *Sum-CSH-CHS* on compressive strength and grinding duration is shown exemplarily in Figs. 6 and 7. It changes for both examples with increasing hydration time. For a constant grinding time *Amorphous* shows significant regions. After one

day of hydration the compressive strength has the highest values with comparable low values of *Amorphous* for one hour grinding duration. With longer hydration time the dependency changes in the other direction and the compressive strength is increasing with the weight fraction of amorphous material in the sample. This clarifies the relation of *Amorphous* and the product quality, which is in this case dependent on the compressive strength. With increasing *Amorphous*, the compressive strength and therefore also the product quality is increasing.

The relation between the compressive strength and the parameter *Sum-CSH-CHS* is less strong. The groups of different grinding durations are located closer to each other. After one day of hydration there is a slight relation of decreasing values of compressive strength for increasing values of *Sum-CSH-CHS*. For longer hydration time the dependency is clearer, where the compressive strength increases with the share of *Sum-CSH-CHS*. With increasing share of *Sum-CSH-CHS* the fraction of hydraulically active material is increasing and therefore also the compressive strength and the product quality are higher. The step between the grinding duration of one hour and three together with six hours shows that the grinding initially has an influence on the formation of the CHS-phases. At a certain point there is probably no more formation of the CHS-phases and only the packing is changing with further grinding.

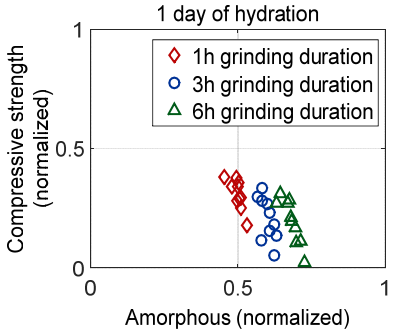

(a)

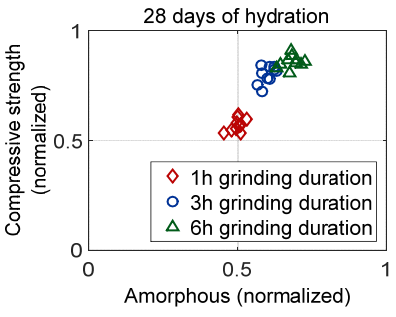

(b)

Fig. 6 Compressive strength over *Amorphous* for (a) one day of hydration time and (b) 28 days of hydration time

Tables I and II summarize the results for the presented parameters. The dependency of the parameters with the drying temperatures and the grinding durations is shown in Table I. Only *Amorphous* and *Alpha* slightly correlate with the drying temperature. The influence of the grinding duration is clearer. The weight fractions of *Amorphous* and *Sum-CSH-CHS* are increasing with longer grinding durations whereas the weight fractions of *Alpha* and *Calcite* are decreasing. The relation of the parameters with the compressive strength and the tensile strength are illustrated in Table II. There is no clear relation after 1 and 2 days of hydration for all parameters, but after 7 and even more after 28 days. The values of the compressive and tensile strength are increasing with *Amorphous* and *Sum-CSH-CHS* and decreasing with the other parameters.

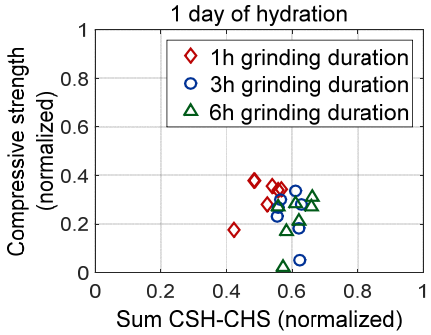

(a)

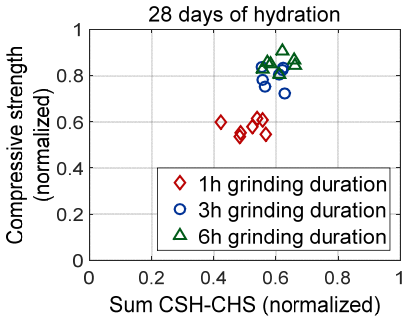

(b)

Fig. 7 Compressive strength over *Sum-CSH-CHS* for (a) one day of hydration time and (b) 28 days of hydration time

TABLE I
DEPENDENCY OF THE PRESENTED PARAMETERS WITH THE DRYING TEMPERATURES AND THE GRINDING DURATIONS

Parameter	Dependency with drying temperature	Dependency with grinding duration
Amorphous	↗	↑
Alpha	Without grinding ↗ With grinding ↘	↓
Calcite	-	0-1h grinding ↗ 3-6h grinding ↓
Sum-CSH-CHS	-	↑

TABLE II
DEPENDENCY OF THE PRESENTED PARAMETERS WITH COMPRESSIVE AND BENDING TENSILE STRENGTH

Parameter	Compressive strength	Bending tensile strength
Amorphous	1-2 days hydration - 7-28 days hydration ↑	1-2 days hydration - 7-28 days hydration ↑
Alpha	1-2 days hydration - 7-28 days hydration ↓	1-2 days hydration - 7-28 days hydration ↓
Calcite	1-2 days hydration - 7-28 days hydration ↓	1-2 days hydration - 7-28 days hydration ↘
Sum-CSH-CHS	1-2 days hydration - 7-28 days hydration ↑	-

B. Calibration Models of NIR-Spectra

The calibration models are calculated for the parameters with different data pre-treatment methods, different combinations of the divided four spectral ranges and for several model orders. Each calibration model is validated with cross validation and the resultant coefficient of determination is determined. Finally, the best combination is selected. In the next paragraphs, the calibration models for the introduced parameters are demonstrated. Additionally, the result of the application of the calibration models of *Amorphous* on unknown data-sets is shown.

Fig. 8 shows the result of the cross-validation and the calibration model for the parameter *Amorphous*. The best combination of the data pre-treatment methods for this parameter is the column-centering as the mandatory and the first derivation as the optional pre-treatment. The selected model order is two and the best combination of the four spectral ranges can be seen in Fig. 8 (b). With this calibration model a coefficient of determination of 97.7% could be reached in the cross validation. The deviations between the calculated values from the NIR-spectra and the directly measured values are decreasing with the grinding duration (Fig. 8 (a)).

Two examples of the application of this calibration model to unknown data are illustrated in Fig. 9. The data of Fig. 9 (a) are from samples grinded in a small laboratory mill for different grinding durations. It can be seen that the deviation between the measured and the calculated values is higher for values greater than 0.75 *Amorphous*. This is most likely a result of the extrapolation of the calibration model calculated with calibration values smaller than 0.75, which is not possible with PLSR. The new test data set has also normalized values between 0.75 and 0.88 of *Amorphous*. Therefore, for these values the occurring deviations are higher. In Fig. 9 (b) the calibration model is applied to a mixed data set of very different samples. Some calculations are very close to the measured values and some have higher deviations. This shows that a big standard data set for calculating the calibration model for the online measurement system will be needed. A broad range of parameter variation is necessary as well as data of different materials for a robust calibration model.

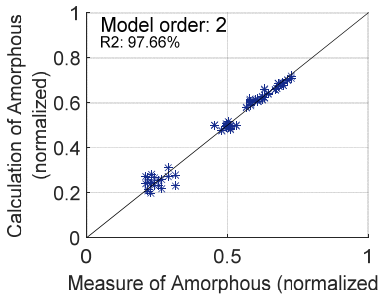

(a)

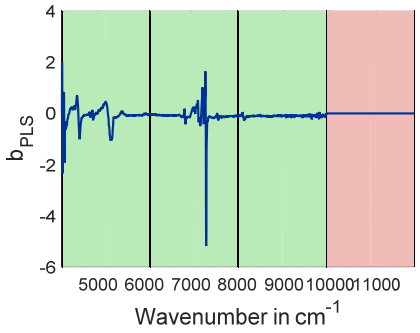

(b)

Fig. 8 (a) The result of the cross-validation and (b) the calibration model of *Amorphous*

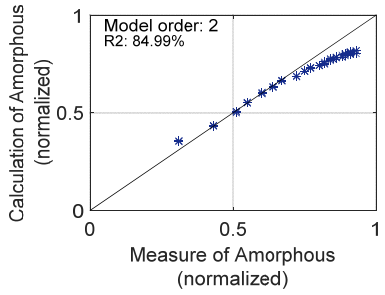

(a)

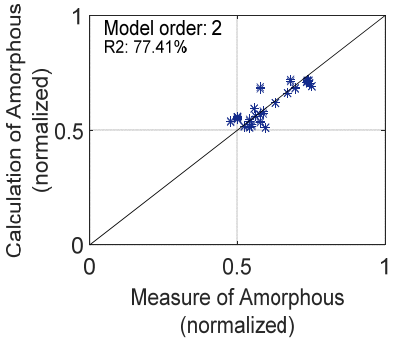

(b)

Fig. 9 (a) Application of the calibration model of *Amorphous* to a measurement series with a small mill and (b) to mixed data

As explained in Section II, it is also feasible for some

parameters to calculate the conversion rate with the calibration model instead of the absolute values. Therefore, the calibration model is determined with the parameters conversion rate over the grinding duration of the training data set (Fig. 10). The best combination of the pre-treatment methods, the combination of the spectral ranges and as well the model order are the same in the calibration model with the conversion rate as for the calibration model with the absolute values. The result of the cross validation (Fig. 10 (a)) points out, that the values of the conversion rate are predominantly represented in the region between -30 to -10 %.

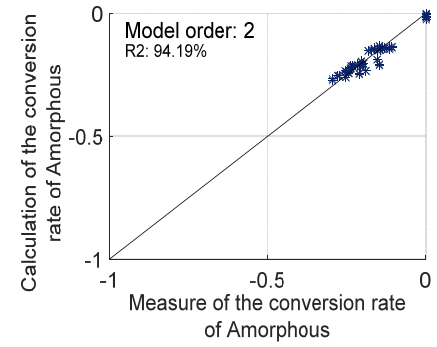

(a)

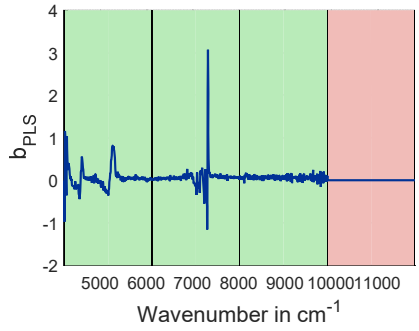

(b)

Fig. 10 (a) The result of the cross-validation and (b) the calibration model of the conversion rate of *Amorphous*

Using this calibration model, the conversion rate of the parameter can be calculated directly from the NIR-spectrum and it is also possible to recalculate the conversion rate to absolute values if the initial value is known. Fig. 11 shows both the calculated conversion rate (a) and the recalculated absolute values of *Amorphous* (b). It can be seen that the deviations for the conversion rate occur in a different range of the diagram compared to the calculated absolute values in Fig. 9 (a). This effect is a result of the calculation of the conversion rate and the initial values. In the calibration data set for example a normalized value of *Amorphous* of 0.6 corresponds to a conversion rate of -21.5% and for the application data set to a conversion rate of -16%. In total the conversion rate varies between 0 and -29.5% corresponding to absolute normalized values of *Amorphous* of 0.21 to 0.725 for the calibration data set. For the application data the conversion rate varies between 0 and -34% with absolute normalized values of *Amorphous* between 0.31 and 0.93. Therefore, the estimation of values in the region of higher values of *Amorphous* is better than the calculation using the calibration model of the absolute values. For example, while the calculation of the conversion rate leads to a recalculated absolute normalized value of around 0.873, the calculation of the parameter with the calibration model calculated with absolute values leads to around 0.785 for a measured absolute normalized value of 0.858 *Amorphous*. So the from the spectra calculated values, which are outside the calibration range can in this case still be estimated by the calibration model of the conversion rate. Which calibration model leads to better results, depends on the calibration and applied data and needs to be tested and validated for each parameter individually.

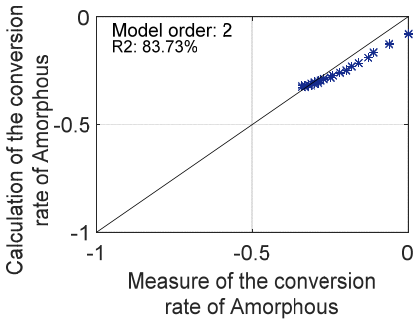

(a)

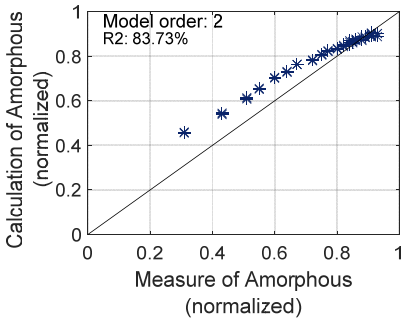

(b)

Fig. 11 (a) Application of the calibration model of the conversion rate of *Amorphous* and (b) the recalculated absolute values of *Amorphous* for the data series, grinded in the small mill

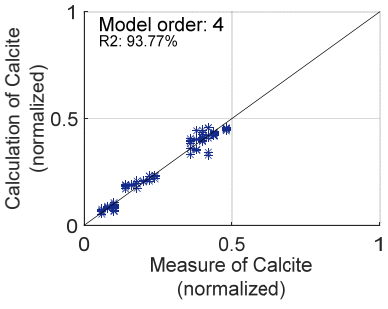

(a)

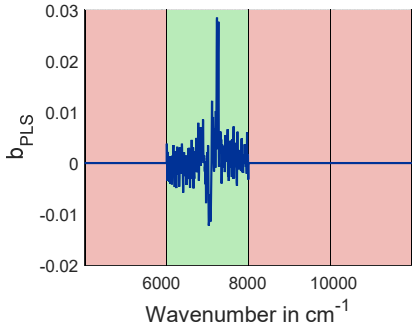

(b)

Fig. 12 (a) The result of the cross-validation and (b) the calibration model of *Calcite*

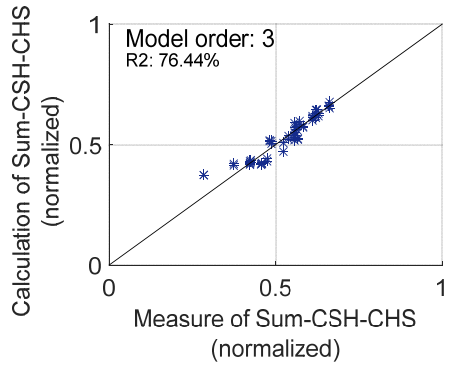

(a)

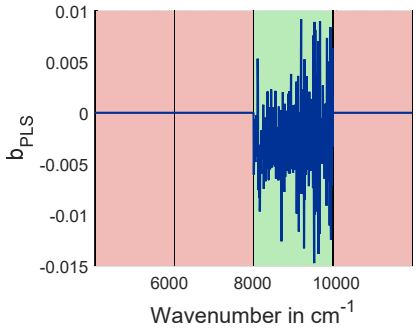

(b)

Fig. 13 (a) The result of the cross-validation and (b) the calibration model of *Sum-CSH-CHS*

For the calculation of the calibration model of *Calcite* only the second spectral range is used (Fig. 12 (b)). The best combination of the data pre-treatment methods is column-centering as the mandatory and the first derivation together with the standard normal variate transformation as the optional pre-treatment steps. With a model order of four, a coefficient of determination of about 93.8% is obtained, where higher values have larger deviations than small ones.

The calibration model for the parameter *Sum-CSH-CHS,* shown in Fig. 13, is not as good as the calibration models for the XRD-parameters, but with a coefficient of determination of 76.4% it is still feasible. The ranking of the different combinations of data pre-treatment is shown in Table III. The selected combination of data pre-treatment is column-centering and first derivation plus SNV transformation. A coefficient of determination of 73.6% can already be reached by a model order of only two. It increases with increasing model order reaching 79.3% with model order six. However, due to the small improvement, model order three is chosen. For validation, the application to new data sets still needs to be tested for this parameter.

TABLE III
RANKING OF THE DATA PRE-TREATMENT METHODS FOR *SUM-CSH-CHS*

Pre-treatment methods	Best model order	R^2
Column-centered, 1. derivation, MA, SNV	2	73.6
Column-centered, 1. derivation, MA, row-centered	2	71.4
MSC, 1. derivation, SNV	2	64.5
MSC, 1. derivation	2	64.4
MSC, 1. derivation, row-centered	2	64.4
Column-centered, 1. derivation, SNV	3	76.4
MSC, 1. derivation, MA, row-centered	3	71.1
MSC, 1. derivation, MA, SNV	3	71.1
MSC, 1. derivation, MA	3	70.7
MSC, SNV	5	73.2
MSC	5	72.1
MSC, row-centered	5	71.6
Column-centered, SNV	6	79.3
Column-centered, 1. derivation, MA	7	69.6
Column-centered, row-centered	9	75.1
Column-centered	9	74.1
Column-centered, 1. derivation, row-centered	10	79.3
Column-centered, 1. derivation	10	78.5

V. CONCLUSION

The monitoring of the product quality during the manufacturing process of Celitement is a challenging task. For the development of a suitable estimation of the product quality based on fast NIR-spectroscopy, different parameters have to be identified. Initially three parameters measured by XRD and one parameter analyzed with thermogravimetry are presented. Different dependencies of the parameters on drying temperature and grinding duration as well as compressive strength could be observed. The dependency of the presented parameters on drying temperature and grinding duration is given in Table I while Table II summarizes the results for the reliance of the parameters with the compressive strength and the tensile strength, respectively. Overall, most parameters show a strong relation to the grinding duration, but only a slight or even no dependency with the drying temperature. Differences in the product quality only occurred for very low and very high drying temperatures meaning there is a broad range for the design of the drying process. The grinding process still needs to be further analyzed in order to achieve the optimal balance between product quality and energy efficiency during the activation process.

Calibration models with good results regarding cross-validation and coefficient of determination were calculated for

all parameters. Calibration models for XRD parameters are generally better than those for parameters from thermogravimetry, but overall all results are feasible. Some calibration models were also tested by an application to unknown data sets. The calibration model or rather its application can be improved by enlarging parameter ranges and by using the conversion rate rather than absolute values for different raw materials.

For the calculation of robust calibration models various data sets from different raw materials with different initial parameter values will be compiled before the appliance in an online measurement system.

REFERENCES

[1] J. GJ. Olivier, "Trends in global CO_2 emissions: 2014 Report," *Hague: PBL Netherlands Environmental Assessment Agency*, 2014.
[2] Celitement GmbH, http://www.Celitement.de/en/, (retrieved 20th of July 2015).
[3] P. Stemmermann, U. Schweike, K. Garbev and G. Beuchle, "Celitement – a sustainable prospect for the cement," *Cement International*, pp. 52-66, 2010.
[4] G. Beuchle, P. Stemmermann, U. Schweike, K. Garbev, "Single-phase hydraulic binder, methods for the production thereof and building material produced therewith," *Grant*, 2008.
[5] Forschungsvereinigung Verein Deutscher Zementwerke e.V.: AiF Forschungsvorhaben Nr.:1 7397N - Anwendung der quantitativen Röntgenbeugungsanalyse in der Qualitätskontrolle von Zementen. Februar 2012 - Oktober 2014.
[6] Bruker Corporation, http://www.bruker.com/, (retrieved 25th of September 2014).
[7] D.A. Burns, and E.W. Ciurczak, "Handbook of near-infrared analysis," *Marcel Dekker*, New York, 1992.
[8] Bruker Optik GmbH, "OPUS Spectroscopy Software - User Manual Quant," *Bruker Optik GmbH*, Ettlingen, 2006.
[9] R.J. Barnes, M.S. Dhanoa, and S.J. Lister, "Standard Normal Variate Transformation and De-trending of Near-Infrared Diffuse Reflectance Spectra," *Applied Spectroscopy*, 5, Vol. 43, 1989.
[10] C. Lutz, J. Matthes, P. Waibel, U. Precht, U. Schweike, G. Beuchle, K. Garbev, P. Stemmermann and H. B. Keller, "Near-infrared spectroscopy for prediction of auxiliary quantities to characterize the product quality of a novel cementitious material," *Materials Characterisation VII*, 90, pp.183-194, 2015.
[11] H. Martens, and T. Naes, "Multivariate calibration," *Chichester: Wiley*, 1989.
[12] D. D. Ruscio, "A weighted view on the partial least-squares algorithm," *Automatica*, Vol. 36, 6, 2000.
[13] DIN EN 12390-2: 2009-08–Prüfung von Festbeton–Teil 2: Herstellung und Lagerung von Probekörpern für Festigkeitsprüfungen. Dtsch. Fass. EN (2009): 12390-2.